

# Bounds on Phonon-mediated Hydrodynamic Transport in a Type-I Weyl Semimetal

Joan Bernabeu

*Departamento de Física de la Materia Condensada,  
Universidad Autónoma de Madrid, Cantoblanco, E-28049 Madrid, Spain\**

Alberto Cortijo

*Departamento de Física de la Materia Condensada,  
Universidad Autónoma de Madrid, Cantoblanco, E-28049 Madrid, Spain\* and  
Condensed Matter Physics Center (IFIMAC), Cantoblanco, E-28049 Madrid, Spain†*

(Dated: November 14, 2023)

We analyze from a microscopic point of view the thermoelectric transport properties of a type-I Weyl semimetal driven by electron-electron interactions mediated by virtual phonons, particularly the feasibility of entering a hydrodynamic regime. Considering also the effects of impurities and the absorption/emission of real phonons, electric and thermal conductivities are obtained. At temperatures  $T$  above the Bloch-Grüneisen temperature  $T_{\text{BG}}$ , virtual phonons behave similarly to real phonons, but the Lorenz ratio is modified by a constant prefactor dependent on the Fermi surface geometry. For temperatures below  $T_{\text{BG}}$ , virtual phonons induce a  $T^2$  dependence in the resistivities, opening a window where momentum-conserving interactions could dominate transport signatures. We find that the onset of such a hydrodynamic regime requires impurity scattering whose inverse relaxation time is one or two orders of magnitude smaller than realistic values, depending on the electron-phonon coupling strength.

## I. INTRODUCTION

Despite having been originally postulated decades ago [1, 2], electron hydrodynamics has become of interest in recent years in light of experimental observations hinting such behavior. In contrast to the conventional diffusive dynamics of electrons in a Drude-like regime, the hydrodynamic regime in an electron system is characterized qualitatively by momentum-conserving electron-electron interactions providing the shortest scattering time.

Recent experiments [3–8] have focused in part on measuring the thermoelectric transport signatures within this hydrodynamic regime, particularly the electric conductivity  $\sigma$  and the thermal conductivity  $\kappa$ , where in principle each one can be proportional to different relaxation times,  $\tau_\sigma$  and  $\tau_\kappa$  respectively. In systems where electric and thermal conductivities have the same characteristic scattering time, the Lorenz ratio  $L \equiv \kappa/(T\sigma)$  acquires a constant value  $L_0$  independent of the temperature  $T$  (and any particular characteristic scale in the system). This is known as the Wiedemann-Franz (WF) law and is the prevalent case for most metals. For systems where  $\tau_\sigma$  and  $\tau_\kappa$  are different, the Lorenz ratio  $L \propto \tau_\kappa/\tau_\sigma$  no longer satisfies the WF law. Electronic systems in the hydrodynamic regime fall into the latter category as  $\tau_{\sigma,e-e} \neq \tau_{\kappa,e-e}$  since the local electric current is relaxed only by processes that do not conserve the flow of the quasiparticles.

The violation the WF law observed in several materials, particularly some type-II Weyl semimetals (WSM) such as  $\text{WP}_2$  [4, 5] and  $\text{Co}_2\text{MnAl}$  [9], has been suggested as a signature of such hydrodynamic regime,

with phonon-mediated electron-electron interactions being proposed as the culprit for such behavior. This suggestion is supported by several studies from first-principles calculations [7, 8, 10, 11] in several type-II WSMs that appear to show regions where the smallest relaxation time is the one associated to phonon-mediated scattering. Anisotropy of the Fermi surface in these type-II WSMs has been suggested [10] as the driving factor enhancing this mechanism. It is of note that in these works, Coulomb scattering is seen to be the least effective scattering processes for the studied materials.

Regarding the WF law, it is imperative to bear in mind that momentum-relaxing interactions between electrons and (real) phonons by themselves might lead to its violation without entering in a hydrodynamic regime. For instance, in three dimensional Fermi liquids where phonon absorption and emission by electrons are the dominant scattering processes at low temperatures, one expects  $\tau_{\sigma,e-e} \propto T^{-5}$  whereas  $\tau_{\kappa,e-e} \propto T^{-3}$ , leading to a clearly nonconstant  $L \propto T^2$ , but no hydrodynamic regime, as phonon absorption and emission processes fail to conserve electron momentum [12]. Similar results can be expected in the bulk of a Weyl semimetal, with some deviations due to surface effects [13]. Nevertheless, most of the theoretical approaches to the problem still consider absorption and emission of real phonons as the primary scattering mechanism for electrons, but with the phonon gas slightly out of equilibrium and thus conserving the total momentum of the electron-phonon fluid in absence of umklapp scattering [14, 15]. Experiments in  $\text{WP}_2$  show however that the violation of the WF law is stronger than expected by electron-phonon scattering alone [4], with the contribution of electron-electron scattering being noticeably different from that of other metals [5].

In the present work we consider the role of electron-

\* joan.bernabeu@uam.es

† alberto.cortijo@uam.es

electron interactions in thermoelectric transport with virtual phonons playing the role of mediators instead of the conventional Coulomb interaction in type-I Weyl SMs. These are clearly different systems to the type-II SMs where potential signatures of hydrodynamics have been observed exclusively thus far. Evidence of hydrodynamics has also been reported in PdCoO<sub>2</sub>, which is not a WSM [3]). Nevertheless, there has been extensive theoretical work based on the premise that a particular instance of a type-I SM may indeed harbor (relativistic) hydrodynamic behavior [16–25]. It is thus of interest to ask whether a system where processes derived from electron-phonon interactions dominate over Coulomb scattering. In the process, we elucidate the general behavior of these scattering processes, whose microscopic treatment is seemingly absent in the literature, and how it entangles with the features of a type-I Weyl SM, finding their imprint on thermoelectric transport and in particular, the WF law.

Let us summarize our results. First of all, there is a characteristic temperature scale, the Bloch-Grüneisen temperature,  $T_{\text{BG}}$ , delimiting two temperature regimes. Such temperature scale also appears in models that only consider phonon emission/absorption [12, 15]. In this work we assume that the Debye temperature  $T_{\text{D}} > T_{\text{BG}}$ , as is the case for metals with small Fermi momenta  $p_f$ .

Above  $T_{\text{BG}}$ , virtual phonon effects are non-negligible when the phonon linewidth  $\Gamma$  is dominated by the effects of the phonon-electron interaction. In this regime electronic scattering times are equal to those of phonon emission and absorption as the virtual phonons act like on-shell real phonons, with quantum interference effects becoming negligible, but the Lorenz ratio acquires a constant value different from  $L_0$ . When there are stronger decay channels for phonons than those provided by the interaction with electrons, then the effects of electron scattering in this temperature regime are suppressed and  $L = L_0$ .

For temperatures below  $T_{\text{BG}}$ , phonons no longer act on-shell as they are not thermally activated, and the quantum fermionic interference between different scattering channels becomes non-negligible. For a simple quadratic band model, this would lead to the effects of electron scattering by virtual phonons being suppressed with respect to the phonon emission/absorption and scattering off impurities. Fundamentally, the wavefunction overlaps associated with the scattering of the Weyl quasiparticles make the contribution of phonon-mediated electron scattering non-negligible. This results in  $\tau_{e-e} \propto T^{-2}$  relaxation times, opening up a parameter window for which electron scattering can dominate over scattering with real phonons for small enough temperatures. Nevertheless, we predict that the onset of a hydrodynamic regime is foiled for realistic electron-phonon coupling strengths and impurity scattering, the latter of which is expected to start dominating at higher temperatures of the order  $T \sim 0.1T_{\text{BG}}$ .

## II. THE MODEL

### A. Particles

We consider the electron dynamics in a WSM described by the following two-band Hamiltonian [26, 27]

$$H_0 = \int_{\mathbf{p}} \psi_{\mathbf{p}}^\dagger [\boldsymbol{\sigma} \cdot \mathbf{d}(\mathbf{p})] \psi_{\mathbf{p}}, \quad (1)$$

where  $\psi_{\mathbf{p}}$  is a two-component spinor, and  $\int_{\mathbf{p}} \equiv \int \frac{d^3p}{(2\pi)^3}$ . A simple diagonalization of the Hamiltonian shows that there are positive and negative energy eigenstates whose energies are given by  $\epsilon_{\pm, \mathbf{p}} = \pm d(\mathbf{p}) \equiv \sqrt{|\mathbf{d}(\mathbf{p})|^2}$ . In particular, we set

$$\mathbf{d}(\mathbf{p}) = v_0 \left( p_x, p_y, \frac{1}{2b} (b^2 - p_z^2) \right), \quad (2)$$

so that the Hamiltonian has two isotropic Weyl nodes (valleys) around  $\mathbf{b}_{\pm} = (0, 0, \pm b)$ . For small momenta around these nodes,  $\delta\mathbf{p}_{\pm} \equiv \mathbf{p} - \mathbf{b}_{\pm}$ , one obtains the low energy Hamiltonians, one for each chirality ( $\pm \equiv L/R$ ),

$$\mathcal{H}_{L,R}(\delta\mathbf{p}_{\pm}) = \delta p_{\pm,x} \sigma_x + \delta p_{\pm,y} \sigma_y \pm \delta p_{\pm,z} \sigma_z, \quad (3)$$

where we have set the Fermi velocity  $v_0 \equiv 1$ , as is also done throughout the rest of this work. The nodes are thus separated by a distance  $2b$ . Importantly, we assume that the chemical potential is the same for both valleys, and much larger than the temperature  $T$ . Without loss of generality, we assume that the chemical potential is positive, meaning that the occupied valence band has no impact in the transport properties and can be neglected. In addition we also assume that  $p_f < b \equiv |b|$  as well in order to have a well defined chirality for each valley.

Longitudinal acoustic phonons have on-shell isotropic energies  $\omega_{\mathbf{q}} = c|\mathbf{q}| \equiv cq$ , where  $c$  is the (dimensionless) speed of sound measured in units of  $v_0$ . For realistic WSM it makes sense to assume  $c \sim 10^{-2} \ll 1$  [13, 15, 28, 29]. In the present work phonons interact with electrons through a deformation potential term [12] (neglecting umklapp processes):

$$H_{e\text{-ph}} = \int_{\mathbf{p}, \mathbf{q}} g_{\mathbf{p}+\mathbf{q}, \mathbf{p}}^{\mathbf{q}} (a_{\mathbf{q}} + a_{\mathbf{q}}^\dagger) \psi_{\mathbf{p}+\mathbf{q}}^\dagger \psi_{\mathbf{p}}. \quad (4)$$

The operator  $a_{\mathbf{q}}$  ( $a_{\mathbf{q}}^\dagger$ ) destroy (create) a phonon with momentum  $\mathbf{q}$ , and the electron-phonon coupling is given by

$$g_{\mathbf{p}', \mathbf{p}}^{\mathbf{q}} = \sqrt{\frac{U}{2\omega_{\mathbf{q}}}} (\mathbf{p}' - \mathbf{p}) \cdot \hat{\mathbf{q}}, \quad (5)$$

where  $U$  is some constant regulating the strength of the electron-phonon interaction that has dimension of energy<sup>-2</sup> after setting  $\hbar = v_0 = 1$  and  $\hat{\mathbf{q}} = \mathbf{q}/|\mathbf{q}|$ .

When projecting the Hamiltonian term (4) onto the conduction band states of (2), the effective coupling (5) reads

$$g_{\mathbf{p}', \mathbf{p}}^{\text{eff } \mathbf{q}} = g_{\mathbf{p}', \mathbf{p}}^{\mathbf{q}} \langle +\mathbf{p}' | +\mathbf{p} \rangle, \quad (6)$$

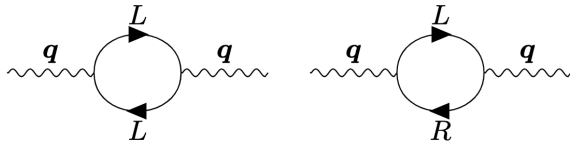


Figure 1. Intravalley and intervalley contributions to the phonon linewidth from the electron-phonon interaction. The bubble diagram with two  $R$  fermions provides the same contribution as the the first diagram.

where the state  $|+\mathbf{p}\rangle$  is the positive energy eigenstate of the Hamiltonian (see Appendix section A). Note that because of overlap term  $\langle +\mathbf{p}'|+\mathbf{p}\rangle$  the effective fermion-phonon coupling is now sensitive to chirality flips in the scattering processes involving different valleys, as can be checked by expressing  $\mathbf{p}'$  and  $\mathbf{p}$  in terms of  $\delta\mathbf{p}_{\pm'}$  and  $\delta\mathbf{p}_{\pm}$ . In the rest of this work, the label  $\mathbf{p}$  will be used instead of  $\delta\mathbf{p}_{\pm}$  to refer to the momenta with respect to the Weyl nodes. For chirality-violating processes where confusion could arise, the momentum around the right-handed node will simply be altered as  $\mathbf{p} \rightarrow \mathbf{p} + 2\mathbf{b}$ , setting it to the reference frame of the left-handed node.

The phonon propagator is given by

$$\mathcal{D}(\mathbf{q}, \omega) = \frac{2\omega_{\mathbf{q}}}{\omega^2 - \omega_{\mathbf{q}}^2 + i\omega_{\mathbf{q}}\Gamma_{\mathbf{q}}}. \quad (7)$$

We have included the effects of interactions through a small but non-vanishing phonon linewidth  $\Gamma_{\mathbf{q}} \ll \omega_{\mathbf{q}}$ . Here we focus on the electron-phonon interaction (4) as the dominant source of this phonon linewidth, represented to lowest order in perturbation theory by the diagrams in Fig.(1), i.e.,  $\Gamma_{\mathbf{q}} = \Gamma_{\mathbf{q}}^{\text{e-ph}}$ . In general, other effects like phonon-impurity scattering or anharmonic effects might enhance  $\Gamma_{\mathbf{q}}$ , so we expect for realistic WSMs,

$$\Gamma_{\mathbf{q}} \geq \Gamma_{\mathbf{q}}^{\text{e-ph}}. \quad (8)$$

In particular, one expects for anharmonic interactions to dominate at sufficiently large temperatures. Conversely, for small enough temperatures, particularly in a region close to  $T_{\text{BG}}$ , anharmonic effects may be suppressed with respect to the absorption/emission of phonons. Hence our assumption of  $\Gamma_{\mathbf{q}} = \Gamma_{\mathbf{q}}^{\text{e-ph}}$  may be sensible below and also for a limited temperature range above  $T_{\text{BG}}$ .

## B. Boltzmann Equation

The evolution of the distribution function  $f_{\lambda}(\mathbf{p}, \mathbf{x})$  for the fermionic quasiparticles with chirality  $\lambda = L, R$  is governed by the quantum Boltzmann equation

$$\partial_t f_{\lambda} + \mathbf{F} \cdot \nabla_{\mathbf{p}} f_{\lambda} + \mathbf{v}_{\lambda} \cdot \nabla_{\mathbf{x}} f_{\lambda} = -\mathcal{I}[f_{\lambda}]. \quad (9)$$

where  $\mathbf{F}$  is the external force acting on the particles and  $\mathbf{v}_{\lambda} \equiv \nabla_{\mathbf{p}} \epsilon_{\mathbf{p}} = \hat{\mathbf{p}}$  is the group velocity for linearly dispersive WSMs. Note that the  $\lambda$  dependence of the group velocity is implicitly encoded in the reference point for the momentum  $\mathbf{p}$ . We point out that we are not considering the contribution from the Berry curvature to the velocity, that might lead to anomalous Hall currents, as we are interested in transport responses linear in external applied fields [20, 23, 30, 31]. The collision integral (right hand side of (9)) contains terms arising from the scattering of electrons by impurities, absorption/emission of real phonons and electron-electron interactions:

$$\mathcal{I}[f_{\lambda}] \equiv \mathcal{I}_{\text{imp}}[f_{\lambda}] + \mathcal{I}_{\text{e-ph}}[f_{\lambda}] + \mathcal{I}_{\text{e-e}}[f_{\lambda}]. \quad (10)$$

Electron-electron interactions are the only processes that conserve electron momentum. We do not consider here screened Coulomb interactions, and assume that virtual phonon exchange is the only source of electron-electron interactions.

We also assume that phonons are at thermal equilibrium, following Bose-Einstein distribution,

$$b_0(\omega) = \frac{1}{e^{\beta\omega} - 1}. \quad (11)$$

The electric ( $\mathbf{J}_{\text{E}}$ ) and heat ( $\mathbf{J}_{\text{T}}$ ) currents can be obtained from the solution  $f_{\lambda}$  of (9):

$$\mathbf{J}_{\text{E,T}} \equiv \sum_{\lambda} \int_{\mathbf{p}} q_{\text{E,T}}^{\lambda} \mathbf{v}_{\lambda} f_{\lambda}, \quad (12)$$

where  $q_{\text{E}}^{\lambda} \equiv q_{\text{E}} \equiv e$  and  $q_{\text{T}}^{\lambda} \equiv q_{\text{T}} \equiv (p - p_f)$  are the chirality-independent charges associated to each current, and  $p \equiv |\mathbf{p}|$ .

In thermal equilibrium, fermions follow the Fermi-Dirac distribution

$$f_0 \equiv f_0(p) = \frac{1}{e^{\beta(p-p_f)} + 1}, \quad (13)$$

for which the collision integral (10) and the currents (12) identically vanish. We thus analyze the non-equilibrium perturbative response to small electric fields and thermal gradients. As usual, the nonlinear Boltzmann equation (9) can be linearized by writing  $f_{\lambda} = f_0 + \delta f_{\lambda}$  and keeping only the terms  $\delta f_{\lambda}$  that depend linearly with the external fields. Eq.(9) then becomes

$$\hat{\mathbf{p}} \cdot [e\mathcal{E} - \beta(p - p_f) \nabla T] \beta f_0 [1 - f_0] = -\mathcal{I}[f_0 + \delta f_{\lambda}], \quad (14)$$

where  $\mathcal{E} \equiv \mathbf{E} + \frac{1}{e} \nabla \mu$  is the electrochemical force and  $\nabla T$  the temperature gradient. We also assume that the system size is much larger than any other scale in the problem. In absence of external magnetic fields that trigger anomaly-related phenomena, we expect that  $\delta f_L = \delta f_R \equiv \delta f$  in Eq.(14) so in practice one only needs to study the Boltzmann equation for a single chirality,

even when chirality-flipping processes are taken into account. Due to the form of the LHS of Eq.(14), it is convenient to parametrize  $\delta f$  as

$$\delta f = \beta^2 f_0 [1 - f_0] [\boldsymbol{\mathcal{X}}_{\text{E,T}}(\mathbf{p}) \cdot e\boldsymbol{\mathcal{E}} - \boldsymbol{\mathcal{X}}_{\text{T}}(\mathbf{p}) \cdot \nabla T], \quad (15)$$

where  $\boldsymbol{\mathcal{X}}_{\text{E,T}}$  are dimensionless vector perturbations. Substituting this expression into (14) and separating the electric and thermal contributions, one formally obtains a vector equation

$$\mathbf{S}_{\text{E,T}} = \mathcal{C} \boldsymbol{\mathcal{X}}_{\text{E,T}}, \quad (16)$$

where the source term is defined as  $\mathbf{S}_{\text{E,T}} \equiv \hat{q}_{\text{E,T}} \hat{\mathbf{p}}$ . The quantities  $\hat{q}_{\text{E}} \equiv 1$  and  $\hat{q}_{\text{T}} \equiv \beta(p - p_f)$  are the dimensionless charges for the sources, and the operator  $\mathcal{C}$  on the RHS is the vectorized version of the collision integral acting on the vector functions  $\boldsymbol{\mathcal{X}}_{\text{E,T}}$ . Although isotropy is technically broken in our model through the internodal vector  $\mathbf{b}$ , we assume that the solution is isotropic and hence postulate that  $\boldsymbol{\mathcal{X}}_{\text{E,T}}(\mathbf{p}) = \boldsymbol{\mathcal{X}}_{\text{E,T}}(\epsilon_{\mathbf{p}}) \mathbf{v} = \boldsymbol{\mathcal{X}}_{\text{E,T}}(p) \hat{\mathbf{p}}$ . For isotropic systems, the currents (12) are related to the external fields through the Onsager transport coefficients

$$\begin{pmatrix} \mathbf{J}_{\text{E}} \\ \mathbf{J}_{\text{T}} \end{pmatrix} = \begin{pmatrix} L_{\text{EE}} & L_{\text{ET}} \\ L_{\text{TE}} & L_{\text{TT}} \end{pmatrix} \begin{pmatrix} e\boldsymbol{\mathcal{E}} \\ \nabla T \end{pmatrix}, \quad (17)$$

which for our model read

$$L_{\text{AB}} = \frac{4\beta^2}{3(2\pi)^2} \int dp p^2 f_0 [1 - f_0] q_{\text{A}}(p) \mathcal{X}_{\text{B}}(p). \quad (18)$$

Note that an extra factor of 2 has been introduced to account for the effect of both valleys/chiralities. The electric conductivity as well as the open-circuit and closed-circuit thermal conductivities are respectively defined as

$$\begin{aligned} \sigma &\equiv e^2 L_{\text{EE}}, & \bar{\kappa} &\equiv L_{\text{TT}}, \\ \kappa &\equiv L_{\text{TT}} - \frac{L_{\text{TE}} L_{\text{ET}}}{L_{\text{EE}}}. \end{aligned} \quad (19)$$

The thermopower is given by  $\alpha \equiv e L_{\text{TE}} = e\beta^{-1} L_{\text{ET}}$ , and the latter equality is due to Onsager reciprocity[32].

### C. Variational Approach

To solve Eqs.(16), we make use of the standard variational approach [33–35]. Introducing the inner product

$$(\mathcal{F}, \mathcal{G}) \equiv \int \frac{d^3 p}{(2\pi)^3} \beta f_0(p) [1 - f_0(p)] \mathcal{F}(\mathbf{p}) \cdot \mathcal{G}(\mathbf{p}), \quad (20)$$

the following functional is defined:

$$\mathcal{Q}_{\text{E,T}}[\boldsymbol{\mathcal{X}}_{\text{E,T}}] \equiv (\boldsymbol{\mathcal{X}}_{\text{E,T}}, \mathbf{S}_{\text{E,T}}) - \frac{1}{2} (\boldsymbol{\mathcal{X}}_{\text{E,T}}, \mathcal{C} \boldsymbol{\mathcal{X}}_{\text{E,T}}). \quad (21)$$

Eqs.(16) are then obtained by applying the variational principle on this functional  $\delta \mathcal{Q}_{\text{E,T}} / \delta \boldsymbol{\mathcal{X}}_{\text{E,T}} = 0$ . The issue of solving the Boltzmann equation (14) can hence

be converted into an  $N$ -dimensional algebraic problem by expanding  $\boldsymbol{\mathcal{X}}_{\text{E,T}}$  into an arbitrary functional basis  $\{F^n\}_{n=0}^{N-1}$ , i.e.,  $\boldsymbol{\mathcal{X}}_{\text{E,T}}(p) = \mathbf{x}_{\text{E,T}} \cdot \mathbf{F}(p)$ . Now the Boltzmann equation (16) becomes a linear equation for the vector of unknown coefficients  $\mathbf{x}_{\text{E,T}}$ ,

$$\mathbf{S}_{\text{E,T}} = \mathbf{C} \mathbf{x}_{\text{E,T}}, \quad (22)$$

where the components of the source vector are  $S_{\text{E,T}}^n \equiv (F^n \hat{\mathbf{p}}, \mathbf{S}_{\text{E,T}})$  and the collision matrix components are given by  $C^{nm} \equiv (F^n \hat{\mathbf{p}}, \mathcal{C}[F^m \hat{\mathbf{p}}])$ . The matrix  $\mathbf{C}$  is not to be confused with the electron-phonon coupling  $C$  (5). If  $\mathbf{C}$  is an invertible operator, Eq.(22) has a unique solution and the transport coefficients will read  $L_{\text{AB}} \propto \mathbf{S}_{\text{A}} \mathbf{C}^{-1} \mathbf{S}_{\text{B}}$ . For the conductivities it implies

$$\begin{aligned} \sigma &= \frac{2e^2\beta}{3} \mathbf{S}_{\text{E}}^\dagger \mathbf{C}^{-1} \mathbf{S}_{\text{E}}, & \bar{\kappa} &= \frac{2}{3} \mathbf{S}_{\text{T}}^\dagger \mathbf{C}^{-1} \mathbf{S}_{\text{T}}, \\ \alpha &= \frac{2e\beta}{3} \mathbf{S}_{\text{E}}^\dagger \mathbf{C}^{-1} \mathbf{S}_{\text{T}} = \frac{2e\beta}{3} \mathbf{S}_{\text{T}}^\dagger \mathbf{C}^{-1} \mathbf{S}_{\text{E}}. \end{aligned} \quad (23)$$

Again, the latter equality in (23) is just the well-known Onsager reciprocity. In the case at hand, it easily proven using (22) and the hermiticity of  $\mathbf{C}$ .

The expressions in (23) are meaningful if the collision matrix is invertible as it happens when momentum-relaxing processes are considered. However, in the presence of exclusively momentum-conserving processes (that also conserve chirality, as we will see later)  $\mathbf{C}$  would have a zero-mode associated with momentum conservation and given by the function  $F^0(p) = \beta p$ . In such a scenario the conductivities (23) would be infinite with the electric field/thermal gradient accelerating electrons indefinitely, preventing any steady state. This is indeed the case for the electric conductivity  $\sigma$ , where a net movement of the electron fluid is needed to carry charge between electrodes, but not necessarily for the thermal conductivity  $\kappa$ , measured in short-circuit conditions. In this short-circuit scenario, heat can be transferred among electronic degrees of freedom without the need of a net fluid movement, so it is expected to be finite even for a purely momentum-conserving system.

Since  $\mathbf{C}_{\text{e-e}}$  is hermitian, it can be diagonalized through an orthogonal basis  $\{F^n\}_{n=0}^{N-1}$ , where  $F^0(p) = \beta p$  is the zero-mode described above. If a small momentum-relaxing perturbation to the total collision matrix of the form  $\tau_{\text{mr}}^{-1} \mathbf{1}$  is introduced so that  $\mathbf{C} = \tau_{\text{mr}}^{-1} \mathbf{1} + \mathbf{C}_{\text{e-e}}$ , then its inverse is given by

$$\mathbf{C}^{-1} = \begin{pmatrix} \tau_{\text{mr}} & 0 & \dots \\ 0 & (\tau_{\text{mr}}^{-1} + \tau_1^{-1})^{-1} & \dots \\ \vdots & \vdots & \ddots \end{pmatrix}, \quad (24)$$

where  $\tau_n^{-1}$  is the eigenvalue corresponding to the basis function  $F^n$ . Plugging this into the equation for the electric conductivity (23) and taking the momentum conserving limit  $\tau_{\text{mr}} \gg \tau_n$  (which is relevant for studying hydrodynamic effects) one obtains

$$\sigma \propto \tau_{\text{mr}} (S_{\text{E}}^0)^2, \quad (25)$$

which in the  $\tau_{\text{mr}} \rightarrow \infty$  limit is infinite, as expected. In our case where  $p_f \gg T$ , one can go further by noticing that at leading order, the zero-mode in the functional basis is related to the source term  $\mathbf{p} \approx p_f \mathbf{S}_E$ . Since the zero-mode  $F^0(p)$  is orthogonal to all other basis vectors,  $0 = P^n \approx S_E^n$  for all  $n > 0$ . Plugging this into Eq.(19), the expression in Eq.(25) is automatically recovered, independently of the hierarchy of  $\tau_{\text{mr}}$  with respect to  $\tau_n$ .

In the case of  $\kappa$ , one can plug in Eq.(23) into the definition given in Eq.(19) and find that  $\kappa \propto \sigma^{-1} \text{Tr} \left[ (\boldsymbol{\Sigma} \mathbf{C}^{-1})^2 \right]$ , where  $\Sigma^{ij} \equiv S_E^i S_T^j - S_T^i S_E^j$ . Since  $\boldsymbol{\Sigma}$  is antisymmetric, the only possibly non-convergent term in the large  $\tau_{\text{mr}}$  limit, which is proportional  $[C^{-1,00}]^2 = \tau_{\text{mr}}^2$ , vanishes. In fact, only terms in the trace proportional to  $\tau_{\text{mr}}$  survive in the momentum-conserving limit since the electrical conductivity  $\sigma \propto \tau_{\text{mr}}$  in the denominator renders their contribution finite. The resulting expression for  $\kappa$  in the momentum-conserving limit is

$$\kappa \propto \sum_{n=1}^{N-1} \tau_n \left( S_T^n - \frac{S_T^0}{S_E^0} S_E^n \right)^2. \quad (26)$$

In our model,  $\mathbf{S}_T = \mathbf{p} - p_f \mathbf{S}_E$ , where  $\mathbf{p}$  is the zero-mode. Using again that  $P^n = 0$  for  $n > 0$ , the thermal conductivity can be expressed as

$$\kappa = \frac{2}{3} \left( \frac{P^0}{S_E^0} \right)^2 \bar{\mathbf{S}}_E^\dagger \bar{\mathbf{C}}^{-1} \bar{\mathbf{S}}_E, \quad (27)$$

where the  $\bar{\mathbf{S}}_E$  and  $\bar{\mathbf{C}}$  are the respective projections of  $\mathbf{S}_E$  and  $\mathbf{C}$  into the subspace orthogonal to the zero mode, where  $\bar{\mathbf{C}}$  is invertible. Eq.(27) is independent of the basis chosen for the subspace orthogonal to the zero mode. Physically speaking, momentum-conserving effects are projected out as they are irrelevant for the short-circuited system where  $\kappa$  is measured. The expression for the thermal conductivity (27) is valid for any system described by a Dirac Hamiltonian such as graphene. A similarly simple expression can be derived for systems with a quadratic dispersion relation, where  $\mathbf{S}_E \propto \mathbf{p}$ .

The discussion in the preceding paragraphs is generic and qualitative. To derive quantitative results for the thermoelectric conductivities, it is necessary to adopt a concrete set of basis functions. For our purposes, it is enough to choose  $\{F^n\}_{n=0}^1$  with

$$F^0(p) = \beta p, \quad F^1(p) = 1. \quad (28)$$

As just argued,  $F^0(p)$  is useful to distinguish momentum-relaxing and momentum-conserving effects in the momentum-conserving limit. In our model, we consider just one further basis function  $F^1$ , from which the perpendicular subspace to  $F^0$  needed to calculate  $\kappa$  (27) can be extracted through the Gram-Schmidt method. In the Fermi liquid regime  $p_f \gg T$ , other functions are not needed, as they only contribute with subleading terms in the Sommerfeld expansion with the small parameter

$(\beta p_f)^{-1}$ . This implies that the result (27) is in fact exact at leading order in  $T/p_f$  using only the basis (28).

#### D. Impurities and Thermal Phonons

Returning to our model, electrons can interact with impurities in the material, real phonons through emission and absorption, and other electrons through virtual phonons (10). Impurities are considered through a relaxation time approximation (RTA),

$$\mathcal{I}_{\text{imp}}[f] \equiv -\frac{\delta f}{\tau_{\text{imp}}}, \quad (29)$$

i.e., the strength of impurity scattering is accounted for by the parameter  $\tau_{\text{imp}}$ . In the matrix form for the Boltzmann equation given in (22), this is equivalent to  $\mathbf{C}_{\text{imp}} = \tau_{\text{imp}}^{-1} \mathbf{1}$ . This shows that impurities relax all modes equally, implying that, for impurity-collision dominated systems,  $\tau_\sigma = \tau_\kappa$  and non-violation of the WF law.

On the other hand, phonon emission and absorption by electrons is a well-known mechanism [12, 33] leading to  $\tau_\sigma \neq \tau_\kappa$  and an explicit violation of the WF law at small temperatures. At large temperatures however, the WF law is restored. Details on the derivation of these conclusions are given in [36]. We also show that, at temperatures above the Bloch-Grüneisen temperature  $T_{\text{BG}}$ ,

$$\tau_{\sigma/\kappa, \text{e-ph}}^{-1} = \beta^{-1} \frac{2(U p_f^2)}{3(2\pi)c^2} \cdot \begin{cases} \frac{5}{2} & \text{if } T \gg T_{\text{BG,W}}, \\ 1 & \text{if } T \ll T_{\text{BG,W}}, \end{cases} \quad (30)$$

where the difference in temperature regimes comes from the fact that for  $T \ll T_{\text{BG,W}} \equiv 2cb$ , chirality-breaking phonon absorption/emission is suppressed as real/thermal phonons do not have enough energy to make the jump between valleys. Here we have defined a second Bloch-Grüneisen temperature  $T_{\text{BG,W}}$  associated to the distance between the two fermion valleys [13]. At temperatures  $T \ll T_{\text{BG}}$  chirality-breaking processes are of course still suppressed but chirality-conserving ones lead to

$$\tau_{\sigma, \text{e-ph}}^{-1} = \beta^{-5} \frac{12g_5 U}{(2\pi)c^6 p_f^2} = \frac{(\beta p_f)^{-2}}{c_2 c^2} \cdot \tau_{\kappa, \text{e-ph}}^{-1}. \quad (31)$$

and the WF law is violated when these relaxation times dominate,  $L/L_0 = \tau_\kappa/\tau_\sigma \neq 1$ . In (31),  $c_2$  and  $g_5$  are numerical constants of order unity, see Appendix section D.

### III. ELECTRON-ELECTRON COLLISIONS

In this section we consider the effects of normal (momentum-conserving) electron-electron interactions mediated by virtual phonons in transport, the primary focus of this work. We first study the collision

integral for intravalley processes  $L, L \rightarrow L, L$ , and then extend it to the full system which also includes the  $R$

node. For intravalley processes the collision integral in the action functional (21) is given by

$$(\mathcal{X}, \mathcal{C}_{e-e} \mathcal{X})^{\text{intra}} = \frac{1}{2} \cdot \frac{1}{4} \beta^2 \int_{\mathbf{p}} \int_{\mathbf{k}} \int_{\mathbf{p}'} \int_{\mathbf{k}'} |M_{LL}^{LL}(\mathbf{p}, \mathbf{k}; \mathbf{p}', \mathbf{k}')|^2 f_0(p) f_0(k) [1 - f_0(p')] [1 - f_0(k')] (2\pi)^4 \delta(p + k - p' - k') \delta^{(3)}(\mathbf{p} + \mathbf{k} - \mathbf{p}' - \mathbf{k}') |\Delta \mathcal{X}|^2, \quad (32)$$

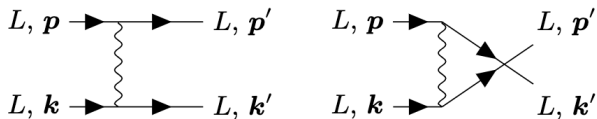


Figure 2. Intranode Feynman diagrams, with the  $t$ -channel corresponding to  $A_t$  (left) and the  $u$ -channel corresponding to  $A_u$  (right).

where  $|\Delta \mathcal{X}|^2 \equiv [\mathcal{X}(p)\hat{\mathbf{p}} + \mathcal{X}(k)\hat{\mathbf{k}} - \mathcal{X}(p')\hat{\mathbf{p}}' - \mathcal{X}(k')\hat{\mathbf{k}}']^2$  and  $|M_{LL}^{LL}(\mathbf{p}, \mathbf{k}; \mathbf{p}', \mathbf{k}')|^2$  is the square of the scattering amplitude for two left-handed fermions with momenta  $\mathbf{p}$  and  $\mathbf{k}$  to scatter to two final electron states with momenta  $\mathbf{p}'$  and  $\mathbf{k}'$  of the same chirality. To see how the action functional collision integral (32) is derived from the collision integral  $\mathcal{I}_{e-e}[f_\lambda]$  appearing in the Boltzmann

equation (10), see section B of [36]. The scattering can occur on two different channels, depending on how the initial states are connected to the final states, as represented via Feynman diagrams in Fig.(2). We call the channel where  $\mathbf{p}$  is connected to  $\mathbf{p}'$  the  $t$ -channel, and the one where  $\mathbf{p}$  is connected to  $\mathbf{k}'$  the  $u$ -channel, following the convention in Quantum Electrodynamics. The scattering amplitude for the  $t$ -channel is given by

$$A_t = -C \frac{q^2}{\omega^2 - \omega_q^2 + i\omega_q \Gamma_q} \langle +\mathbf{p}' | +\mathbf{p} \rangle \langle +\mathbf{k}' | +\mathbf{k} \rangle. \quad (33)$$

Note that since we are considering left chiral states, technically  $|+\mathbf{p}\rangle$  represents  $|+, -\mathbf{b} + \delta\mathbf{p}\rangle$ . Here  $\mathbf{q} \equiv \mathbf{p}' - \mathbf{p} = \mathbf{k} - \mathbf{k}'$  is the virtual phonon momentum and  $\omega \equiv p' - p = k - k'$  is its energy. The  $u$ -channel amplitude is obtained by interchanging  $\mathbf{p}' \leftrightarrow \mathbf{k}'$ . The total scattering amplitude is then given by  $M_{LL}^{LL} \equiv A_t - A_u$ , where the minus sign is due to the fermion exchange from the  $t$  to the  $u$  diagrams. After some manipulations, one finds that

$$(\mathcal{X}, \mathcal{C}_{e-e} \mathcal{X})^{\text{intra}} = \frac{\beta^2}{4(2\pi)^6} \int_0^{q_D} dq \int_{-q}^q d\omega \int_{\frac{q-\omega}{2}}^\infty dp pp' \int_{\frac{q+\omega}{2}}^\infty dk kk' \int_0^{2\pi} d\varphi_{q,pk} |M_{LL}^{LL}|^2 (\beta\omega)^2 b_0(\omega) [1 + b_0(\omega)] f_0(p) [1 - f_0(p)] f_0(k) [1 - f_0(k)] |\Delta \mathcal{X}|^2, \quad (34)$$

where now  $p'$  and  $k'$  should be understood as shorthands for  $p' \equiv p + \omega$  and  $k' \equiv k - \omega$ . A Debye cutoff  $q_D$  to the phonon momentum has been introduced, although it will not have any effect due to the assumption that  $T_{\text{BG}} < T_D$ , which effectively restricts  $q$  to values under  $2p_f < q_D$ . To proceed further analytically, it is necessary to study this integral in asymptotic high and low temperature regimes,  $T \gg T_{\text{BG}}$  and  $T \ll T_{\text{BG}}$  respectively.

### A. High Temperatures

The full square of the scattering amplitude equates to  $|M_{LL}^{LL}|^2 = |A_t|^2 + |A_u|^2 - 2\text{Re}[A_t^* A_u]$ . The  $|A_t|^2$  and  $|A_u|^2$  give identical contributions to the collision integral as can

be seen by relabeling  $\mathbf{p}' \leftrightarrow \mathbf{k}'$  in the original integral (32). These induce term of the form

$$I_\omega \equiv \int_{-1}^1 \frac{f(x)}{[(x-c)^2 + \frac{\Gamma_q^2}{4q^2}][(x+c)^2 + \frac{\Gamma_q^2}{4q^2}]} dx, \quad (35)$$

inside the  $q$  integral, where  $x \equiv \omega/q$  is a dimensionless form of the virtual phonon energy and  $f(x)$  is some function. The residue theorem can be used to perform the integral, with the enclosing curve being far enough from the poles appearing in the denominator of (35). If  $f(x)$  contains no further poles within this contour, then expanding  $f(x)$  in a Taylor series around  $x = 0$  and performing the integral evaluates to

$$I_\omega = \frac{\pi q}{\Gamma_q} \left[ \frac{1}{c^2} f(0) + \frac{1}{2} f''(0) \right] + O(1), \quad (36)$$

where the  $O(1)$  refers to terms that are proportional to a power of 0 or more of the small parameters  $c$  and  $\Gamma_q/(2q)$ . A similar procedure can be carried out for the interference term that depends on  $2\text{Re}[A_t^* A_u]$  (see section B1a of [36]). However, in that case, the results are of a higher-order in the expansion parameters than the non-interference contribution (36), and can thus be neglected.

The next-to leading order term proportional to  $f''(0)$  is considered because the contribution from the leading term proportional to  $f(0)$  is actually vanishing at the leading order in the Sommerfeld expansion, where  $p = k = p' = k' = p_f$  and the  $|\Delta\mathcal{X}|^2$  term in (32) is easily seen to vanish because of momentum conservation. This is not the case for the  $f''(0)$  term, which is non-vanishing at the leading order in the Sommerfeld expansion. This implies that the ratio between the contributions of  $f(0)$  and  $f''(0)$  is of order  $(T/cp_f)^2 \sim (T/T_{\text{BG}})^2$ . Therefore, for temperatures above the Bloch-Grüneisen temperature, the  $f(0)$  term dominates over the one proportional to  $f''(0)$  so, in practice, only the  $f(0)$  term is relevant in this subsection.

The assumption that  $f(x)$  has no other poles inside the contour only applies for  $T \gg T_{\text{BG}}$  as the Fermi-Dirac distribution functions contained in  $f(x)$  also have imaginary poles at the Matsubara frequencies, being the lowest of order  $\beta^{-1} = T$ . Therefore, when  $T \gg T_{\text{BG}}$ , we can integrate along contours not containing Matsubara poles. This is not the case if  $T \lesssim T_{\text{BG}}$ , to be considered in the next subsection. The relevance of the Bloch-Grüneisen temperature will become clear shortly.

Assuming that the dominant contribution to the phonon linewidth comes from electron-phonon interactions, that is, Eq.(8) is an (approximate) equality, one finds that

$$(\mathcal{X}, \mathcal{C}_{e-e} \mathcal{X})^{\text{intra}} = \frac{4c_2(U p_f^2) \beta^{-2}}{3(2\pi)^3 c^2} [X'(p_F) p_f]^2. \quad (37)$$

where  $X(p) \equiv \mathcal{X}(p)/p$  and  $c_2$  is a numeric constant presented previously in (31) and defined in (D1). Expanding  $X(p)$  as a linear combination of the basis functions (28) to extract the matrix components of  $\mathcal{C}_{e-e}$ , only the  $C_{e-e}^{11}$  component is non-zero, as expected from the fact that that  $F^0(p)$  is a zero-mode. For this reason, this collision integral does not contribute to the electric conductivity, again as expected from Eq.(25). On the other hand, it contributes to the thermal conductivity as much as the interaction with real phonons (30),

$$\tau_{\kappa, e-e}^{-1} = \tau_{\kappa, e-ph}^{-1}. \quad (38)$$

In physical terms, this can be understood from the fact that at  $T > T_{\text{BG}}$ , the dominant contribution to the electron-electron collision integral is from virtual phonons satisfying the on-shell condition  $\omega = cq$  stemming from the poles in Eq.(35). It is natural to expect that the processes in fig. (2) share the same time scale as the emission and absorption of real phonons,

$$\tau_{e-e}^{-1} = \tau_{\text{emission}}^{-1} + \tau_{\text{absorption}}^{-1} \equiv \tau_{e-ph}^{-1}.$$

If impurity scattering is negligible (which is natural to expect at sufficiently high temperatures), and ignoring chirality-violating e-e processes, then one sees that

$$L = \frac{L_0}{2}, \quad (39)$$

as the thermal conductivity would now have half the relaxation time of the electric conductivity, oblivious to electron-electron interactions. This equality is only valid when the inequality in Eq.(8) saturates. For any larger phonon linewidth, electron-electron scattering mediated by phonons would be suppressed at  $T > T_{\text{BG}}$ . Physically this corresponds to the scenario where the on-shell virtual phonons, acting like real phonons, have decay channels stronger than those of emission and absorption by electrons, thus suppressing the emission and absorption-dependent processes depicted in Fig.(2). In this limit,  $L \rightarrow L_0$ , independently on whether chirality-violating processes are considered or not.

## B. Low Temperatures

At temperatures below  $T_{\text{BG}}$  the Matsubara poles start to play a role and the approximation in Eq.(36) is no longer valid. Instead of attempting to calculate the contribution of these new poles, we make the observation that, in this regime, the Bose-Einstein distribution in Eq.(34) can no longer be approximated by its  $\beta\omega \rightarrow 0$  limit. We expect then that, for  $T \ll T_{\text{BG}}$ , the equilibrium Bose-Einstein distribution will be the dominating contribution, fixing  $\omega \sim \beta^{-1}$  instead of the on-shell condition  $\omega \sim cq$ . This observation, together with the defining condition for this temperature regime, implies that  $\omega \ll \omega_q$  and hence the  $\omega$  dependence of the propagator in Eq.(7) can be dropped. Consequently the scattering amplitude for the  $t$ -channel becomes

$$\begin{aligned} A_t &= U \frac{q^2}{\omega_q^2} \langle +\mathbf{p}' | +\mathbf{p} \rangle \langle +\mathbf{k}' | +\mathbf{k} \rangle \\ &\simeq \frac{U}{c^2} \langle +\mathbf{p}' | +\mathbf{p} \rangle \langle +\mathbf{k}' | +\mathbf{k} \rangle, \end{aligned} \quad (40)$$

where we have dropped the phonon linewidth  $\Gamma \ll \omega_q$  as it is no longer necessary to make the integral convergent.

In the  $T \gg T_{\text{BG}}$  regime we argued that the interference term in the square of the scattering amplitude could be dropped as it was subleading in the  $c$  and  $\Gamma/(2q)$  expansion stemming from Eq.(36). That statement is no longer valid, as the low temperature approximation for the amplitude Eq.(40) obviously has no poles, and we need to consider the interference contribution from  $-2\text{Re}[A_t^* A_u]$ . The physical intuition for this is that for temperatures above  $T_{\text{BG}}$ , phonons behave classically and quantum interference effect is negligible. For temperatures below

$T_{\text{BG}}$ , phonons regain their quantum behavior and interference terms are no longer subleading. Nevertheless, the simple form of the amplitudes in Eq.(40) makes calculations simple. For instance, one can show that, in the low temperature limit,

$$|M_{LL}^{LL}|^2 = \frac{U^2}{4c^4} (1 - \cos \theta_{pk})^2, \quad (41)$$

where  $\theta_{pk}$  is the angle between  $\mathbf{p}$  and  $\mathbf{k}$ . It is important to note that the equivalent intraband square of the scattering amplitude would vanish in a model diagonal in the electron basis of the Hamiltonian, as then the wavefunction overlaps would be trivial and  $A_t = A_u$  in Eq.(40). This would mean that higher order terms in  $\omega$  would be required for the scattering amplitude, which would suppress the contribution of the collision integral by a power of the small parameter  $T/p_f$  and hence the contribution of electron-electron scattering mediated by phonons to transport effects.

After some intermediate calculations, the collision integral reduces to

$$(\mathcal{X}, \mathcal{C}_{e-e} \mathcal{X})^{\text{intra}} = \frac{2^4 U^2 p_f^7 \beta^{-3}}{35 (2\pi)^5 c^4} [4c_2^2 + 2b_4] X'(p_F)^2, \quad (42)$$

where  $c_2$  and  $b_4$  are  $O(1)$  numeric constants defined in (D1) and (D2). The inverse relaxation time  $\tau_{\kappa, e-e}^{-1}$  will now scale with temperature as  $T^2$ , just like in the case of Coulomb scattering, and with the electron-phonon coupling strength as  $U^2$ . This is to be expected as, in the case of Quantum Electrodynamics, virtual photons are always in the  $T \ll cq$  regime where the  $\omega^2$  in the denominator of the photon propagator is negligible, as in the case Coulomb interaction. The prefactors however are obviously different in the case of Coulomb and virtual phonons.

### C. Chirality-violating processes

Until now we have studied processes within an single Weyl node, valid when interactions do not induce changes in the chirality. In Weyl systems, nodal points come in pairs, as is the case for our starting model Eq.(1), one for left ( $L$ ) and another for right-handed ( $R$ ) Weyl fermions. Therefore, besides the intraband  $(L, L) \rightarrow (L, L)$  scattering processes we had been considering up until now, we should consider  $(L, L) \rightarrow (R, R)$ ,  $(L, R) \rightarrow (L, L)$ ,  $(L, R) \rightarrow (L, R)$  etc. Out of all these possibilities, only the process  $(L, R) \rightarrow (L, R)$  conserves chirality. While the associated collision integral is more complicated due to the anisotropic wavefunction overlaps in the square of the scattering amplitude (Eq. B.48 in the Supplementary Material), the integral is essentially solved in similar fashion to the chirality-conserving situation.

Chirality-violating processes however, are a different story. In the reference frame of one of the nodes and for processes that violate chirality once, such as  $(L, R) \rightarrow$

$(L, L)$ , Dirac deltas associated to momentum conservation in the collision integrals take the form

$$\delta^{(3)}(\mathbf{p} + \mathbf{k} - \mathbf{p}' - \mathbf{k}' \pm 2\mathbf{b}). \quad (43)$$

For processes that violate chirality twice, such as  $(L, L) \rightarrow (R, R)$  we have  $\delta^{(3)}(\mathbf{p} + \mathbf{k} - \mathbf{p}' - \mathbf{k}' \pm 4\mathbf{b})$ . These Dirac deltas are similar to the ones appearing in umklapp processes with a lattice vector  $2\mathbf{b}$  separating two copies of the same Fermi surface. Note however that momentum here is strictly conserved, as can be seen if the momenta are put back into the original reference frame of Eq.(1).

At large temperatures,  $T \gg T_{\text{BG},W}$ , the only relevant poles in the  $\omega$  integral are those provided by the phonon propagator in Eq.(7) so that the expansion in Eq.(36) still holds, making the phonons effectively on-shell. In the limit where the inequality Eq.(8) is saturated, one recovers the result in Eq.(38) and an analogously similar result,

$$(\mathcal{X}_0, \mathcal{C}_{e-e} \mathcal{X}_0)_{\text{h.t.}} = \frac{\beta^4 (4b)^2}{2} \int_{\mathbf{q}} \frac{\Gamma_{e\text{-ph}}^{\text{inter}}(\mathbf{q})}{(\beta\omega_{\mathbf{q}})^2}, \quad (44)$$

where  $\Gamma_{e\text{-ph}}^{\text{inter}}$  is the contribution to the phonon linewidth from a  $L - R$  fermion bubble. This shows how  $\tau_{\sigma, e-e}^{-1}$  is directly related to the linewidth associated to interband processes, which are the only electron scattering processes that can relax the electric current in the system. The contribution to the electric conductivity (44), quadratically dependent on the internodal distance, leads to a Lorenz ratio of the form,

$$L = \frac{1}{2} \left( 1 + \frac{16b^2}{10p_f^2} \right) L_0. \quad (45)$$

For temperatures below  $T_{\text{BG},W}$  but still above  $T_{\text{BG}}$ , electron-electron scattering processes that violate chirality no longer contribute and the Lorenz ratio satisfies the equality in Eq.(39). As in the case of intravalley scattering, this is only valid where the dominant phonon decay channel is associated to scattering with electrons. Otherwise,  $L \rightarrow L_0$ .

At low temperatures, virtual phonons cannot be considered on-shell. Scattering amplitudes for processes that include more than one chirality involve more complicated wavefunction overlaps but otherwise share the relatively similar simple form of Eq.(41) (see section A of the appendix). The integral for the chirality conserving process  $(L, R) \rightarrow (L, R)$  is analogous to the one performed for  $(L, L) \rightarrow (L, L)$  in Eq.(42), whereas the one for chirality-violating processes now includes the momentum conservation delta shown in Eq.(43). This delta, along with the restriction that all electron momenta lie on the Fermi sphere, restricts the available phase space as is the case with umklapp scattering [33, 37]. For  $2b \geq 4p_f$ , these processes are not kinematically allowed. The only interesting parameter space for us to consider is then the

relation  $2p_f < 2b < 4p_f$ , as our model relies on the assumption that  $2p_f < b$ , where chiralities are well defined. While these integrals can be performed analytically, the end result are somewhat complicated expressions of  $b$ , and are written in section B4 of the Supplementary Material [36] for reference. In the end one finds that they also lead to a  $U^2T^2$  scaling for the inverse relaxation times just like the chirality-conserving processes (42). Conversely to that result however, they also contribute to the relaxation of the electric current because of the Umklapp-like nature of (43).

#### IV. DISCUSSION

We have shown how the non-trivial structure of the Weyl Hamiltonian in Eq.(1) had the important consequence of allowing phonon-mediated  $T^2$  inverse relaxation times at low temperatures due to the nontrivial wavefunction overlaps  $\langle +\mathbf{k}' | +\mathbf{k} \rangle$ . It was the key point also in allowing relaxation of electric current through chirality-violating intervalley scattering, having important properties both at  $T > T_{BG}$  with a non-trivial Lorenz ratio (Eq.(45)) as well as low temperatures, as we will discuss further below. Nevertheless, more unique topological properties of the material fail to make an impact, at least in the absence of a quantum anomaly-inducing magnetic field. Its inclusion is left for future work.

Having discussed already the high-temperature behavior in the previous section, we focus here on the properties at temperatures  $T \ll T_{BG}$ , relevant for experimentally observing hydrodynamic signatures. When studying thermoelectric transport in experiments, it is useful to consider the electric and thermal resistivities, which can be conveniently parametrized respectively as

$$\rho \equiv \sigma^{-1} = A_0 + A_2T^2 + A_5T^5, \quad (46)$$

$$WT \equiv TL_0/\kappa = B_0 + B_2T^2 + B_3T^3, \quad (47)$$

following the scaling of the resistivities given in Ref.[5] for WP<sub>2</sub>. While WP<sub>2</sub> is a semimetal with a Fermi surface more complex than the one studied here, similar features in the thermoelectric transport are seen to arise. The resistivities are plotted in Figs.(3a-b) in the absence of impurity scattering. The full Lorenz ratio is plotted in Fig.(3c).

As is clear from our model at low temperatures,  $A_0$  and  $B_0$  are the coefficients associated with impurity scattering,  $A_2$  and  $B_2$  with electron scattering (42), and  $A_5$  and  $B_3$  with thermal phonon emission/absorption by electrons (31). In a system that is at some point dominated by electron-electron interactions, one then expects the Lorenz ratio to level out at the constant value  $L/L_0 = \rho/WT = \tau_{\sigma,e-e}^{-1}/\tau_{\kappa,e-e}^{-1} = A_2/B_2$ . For our model,  $A_2$  is non-vanishing only for  $2b < 4p_f$  as otherwise electric current-relaxing intervalley electron-electron interactions are absent. This leads to the curve plotted in

Fig.(3d), where the ratio  $A_2/B_2$  is plotted as a function of  $2b/p_f$ . It is important to note that this quantity is completely independent of the electron-phonon coupling  $U$  and the phonon velocity  $c$ , and therefore only depends on the geometric factor  $2b/p_f$ . The ratio is expectedly small as intervalley electron-electron scattering contributes much less than the intravalley counterpart present in thermal conduction. However, one would expect that such a ratio could increase for systems with different geometries or carriers [38, 39]. For example, in a compensated (inversion-breaking) Weyl semimetal with an electron band and a hole band (instead of the two electron bands), chirality-conserving  $(L, R) \rightarrow (L, R)$  processes would be able to relax the electron current owing to the fact that the fermions of each valley have group velocities with the opposite sign. Following the procedure of Ref.[40] one can deduce that the ratio  $A_2/B_2$  in such a system takes the form,

$$\frac{A_2}{B_2} = \frac{10\alpha^2 (4305 + 441\alpha^2 - 1980\alpha^4 + 700\alpha^6)}{3 (27090 + 3885\alpha^2 + 63\alpha^4 + 900\alpha^6)}, \quad (48)$$

where  $\alpha = \min[T_D/T_{BG}, 1]$ . In a system with a sufficiently small Fermi surface so that  $T_{BG} < T_D$ , this would lead to a value of  $A_2/B_2 \sim 0.36$ , which is of the same order of the observed values in several materials, see Ref.[5]. In the opposite limit, where  $T_{BG} > T_D$ , then one has  $A_2/B_2 \sim 0.53\alpha^2$ , i.e. the Lorenz ratio can become arbitrarily small. This is a similar conclusion to one reached in Ref.[40], although a screened Coulomb potential is behind that result, whereas Coulomb interactions are expected to be subdominant with respect to electron-phonon interactions in realistic semimetals [7, 8, 10]. Here, by contrast, this result is reached for a constant potential (modulo structure factors) provided by the low temperature phonon-mediated electron-electron processes (41). As in the original model, mixed-chirality processes are essential for a  $T^2$  electric conductivity.

To achieve electron hydrodynamic behavior, electric current-conserving interactions need to dominate over those that relax it. The latter correspond to the relaxation times pertaining to the electric conductivity, i.e. impurities  $\tau_{imp}$ , phonon absorption/emission  $\tau_{\sigma,e-ph}$  and intervalley (Baber) scattering  $\tau_{\sigma,ee}$ . The former correspond to the electron-electron collisions that conserve flow, i.e. intravalley scattering (32), that dominate the electron-electron component of the thermal conductivity,  $\tau_{\kappa,ee}$ , as the collision operator for thermal conduction does not filter out these contributions. This can easily be seen from Fig.(3d); if intervalley scattering dominated the electron-electron contribution to  $\kappa$  as it does for  $\sigma$ , then one would have  $A_2/B_2 \sim 1$ . Fig (3d) clearly indicates this is not the case. Hence, to search for a window for electron hydrodynamic behavior, it is sensible to compare  $\tau_{\kappa,e-e}$  with the electric current-relaxing timescales [5]. The relaxation time associated to the viscosity and stemming from electron-electron interactions should be of this same order, as flow-conserving collisions are not as-

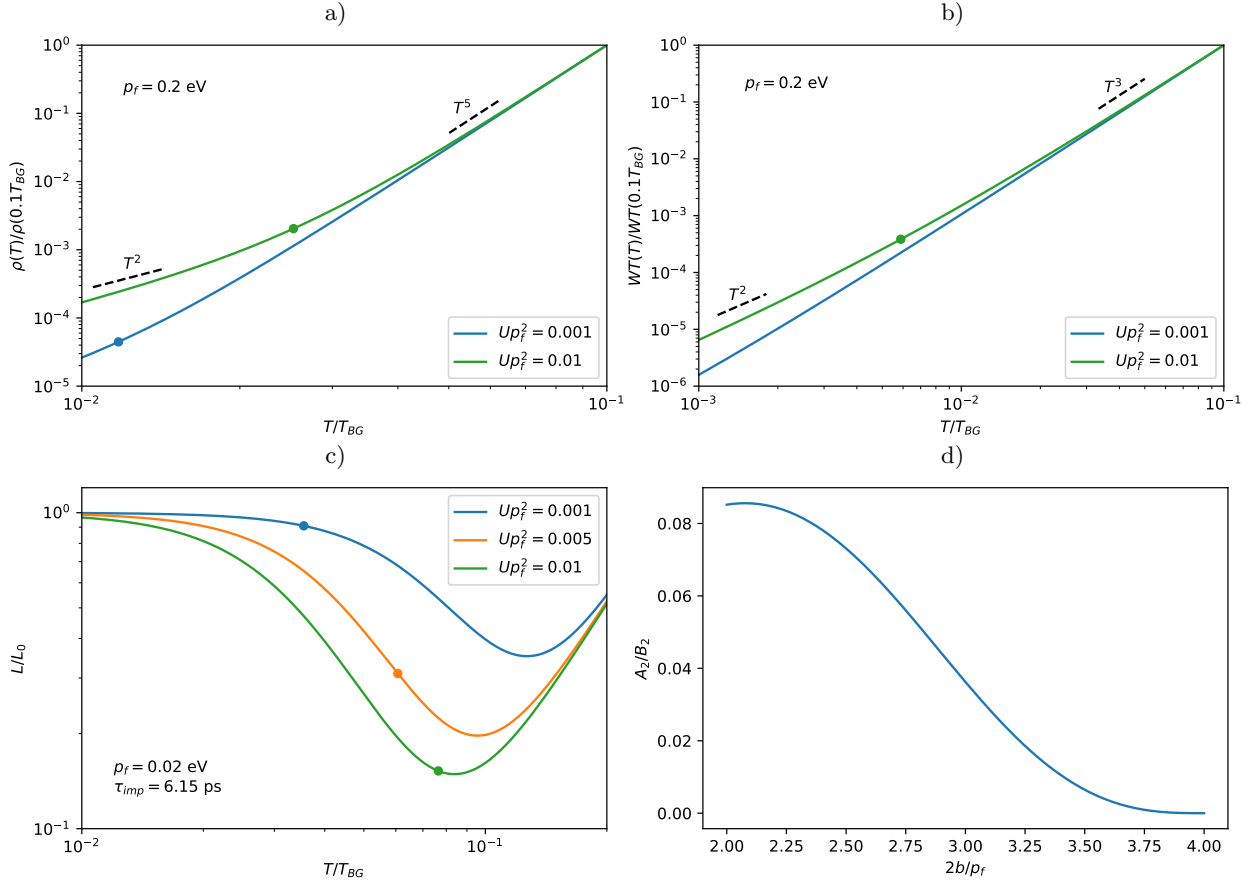


Figure 3. **a** and **b**: Electric (a) and thermal (b) conductivities for  $T \ll T_{\text{BG}}$  for different electron-phonon interaction strengths  $Cp_f^2$ . Points indicate temperature below which electron-electron scattering is stronger than electron-phonon scattering. In the case of the thermal conductivity (b) for the smallest electron-phonon coupling, the point is below the represented temperature scale because the  $T^3$  scaling from absorption/emission of phonons does not decrease as fast as the  $T^5$  scaling from the same source for the electric resistivity. The constant contributions from impurity scattering, i.e.  $A_0$  and  $B_0$  terms in (46, 47) have been omitted to show the onset of the  $T^2$  scaling behavior. **c**: Lorenz ratio at small temperatures  $T \ll T_{\text{BG}}$  for different coupling strengths. Points indicate where current-conserving interactions start dominating over current-relaxing ones (see fig. 4) for temperatures below the point. **d**: Quotient between the  $A_2$  and  $B_2$  terms in (46, 47) which corresponds to the Lorenz ratio of the electron-electron contributions to the resistivities. Plots a-c are drawn for  $p_f = 0.2$  eV and  $c = 0.02v_f$  with an internodal separation is set to  $2b = 3p_f$ . Plot d is independent of these parameters.

sociated to any zero-mode of the collision integral (9) for perturbations from thermal equilibrium proportional to spatial gradients of the flow velocity. With this in mind, the logarithm of the ratio between  $\tau_{\kappa, e-e}^{-1}$  and the electric current inverse relaxation time,  $\tau_{\sigma, e-e}^{-1} + \tau_{\sigma, e-ph}^{-1} + \tau_{\text{imp}}^{-1}$  is plotted in Fig. (4). Hydrodynamic behavior is favored for larger electron-phonon coupling strengths and for a limited temperature window where impurities do not yet dominate. For a typical value of  $\tau_{\text{imp},0} = 6.15$  ps (corresponding to a mean scattering time of  $1.9 \mu\text{m}$  [7] and a Fermi velocity of  $3.09 \cdot 10^5 \text{ ms}^{-1}$  as in  $\text{WTe}_2$  [41]), it is shown in the leftmost plot of Fig.(4) that a hydrodynamic regime is basically inaccessible for the represented parameter ranges. Considering impurity scattering times 10 and 100 times stronger, such a window opens for  $Up_f^2 \gtrsim 0.007$  and  $Up_f^2 \gtrsim 0.003$ , respectively, as is shown in the center and right plots of Fig. (4). Re-

alistic electron phonon-coupling constants in the range  $\lambda \sim 0.1 - 1$  translate to a range  $Up_f^2 \sim 0.0005 - 0.005$  C, which clearly shows that the impurity scattering time needs to be of one or two orders of magnitude larger than the value of  $\tau_{\text{imp},0}^{-1}$  considered for momentum-conserving scattering to be relevant. For example, for the Weyl SM TaAs, the coupling constant for acoustic phonons is  $\lambda \sim 0.34$  [42], which would need impurity relaxation times two orders of magnitude larger than  $\tau_{\text{imp},0}^{-1}$ . It is worth noting that while impurity scattering is a fundamental aspect in predicting electron hydrodynamics, its nature (i.e. short vs long range Coulomb impurities) is not relevant as the possible differences are subleading in the regime  $T/p_f \ll 1$  considered here [43].

As a conclusion, we have described how the Bloch-Grüneisen temperature  $T_{\text{BG}}$  divides the behavior of phonon-mediated electron-electron collisions into two re-

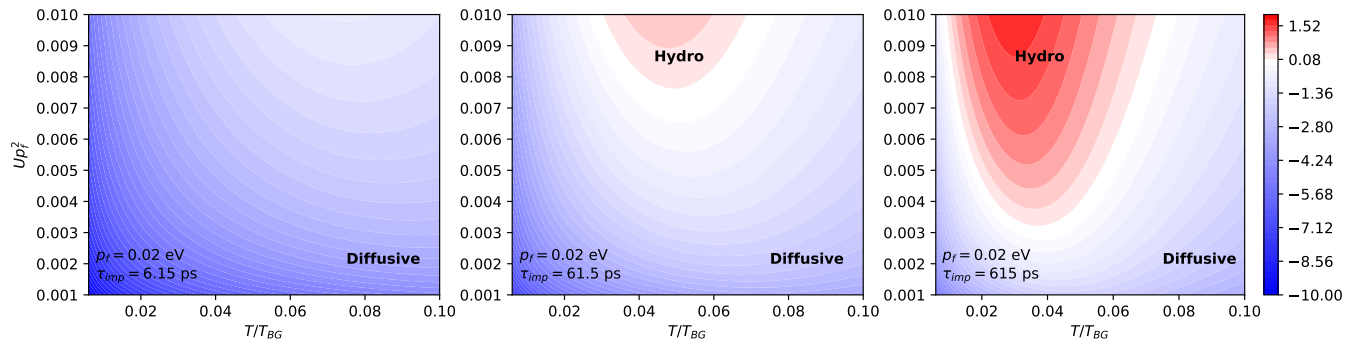


Figure 4. Plot of  $\log\left(\frac{\tau_{\kappa,e-e}^{-1}}{\tau_{\sigma,e-e}^{-1} + \tau_{\sigma,e-ph}^{-1} + \tau_{imp}^{-1}}\right)$  as a function of temperature and electron-phonon coupling strength, plotted from left to right for three different impurity relaxation times,  $\tau_{imp,0} = 6.15$  ps,  $10\tau_{imp,0}$  and  $100\tau_{imp,0}$ . The red region indicates where electric current-conserving interactions dominate, whereas the blue region indicates where current-relaxing interactions with virtual and real phonons, as well as impurities dominate. The latter is labeled "Diffusive", as transport in this region can never be dominated by electric current-conserving collisions, whereas the former is labeled "Hydro" as this is where these collisions might dominate, depending on impurity scattering.

gions as it does for absorption and emission of real phonons. In the case where the phonon interactions are stronger than anharmonic effects, we have seen how at  $T > T_{BG}$  the Lorenz ratio is modified to a multiple of the Lorenz number (39, 44). If phonon decay is driven by other interactions, then the Lorenz ratio in this regime is unaltered. At small temperatures, we have obtained that the electric and thermal resistivities scale as (46) and (47). We concluded that in the simple type-I Weyl SM model studied here with isotropic fermion pockets and electron-phonon interactions a hydrodynamic regime would necessitate highly-pure samples. We speculate then that the anisotropy of the Fermi surface may magnify the effect of electron-electron interactions by an order of magnitude so as to lead to the observable hydrodynamic behavior in real materials, as has been suggested

elsewhere [10]. Nevertheless, our analytical results seem to align qualitatively well with the first principles estimations of the relaxation times. In those, it is seen that for high temperatures electron-electron collisions mediated by phonons contribute as much as absorption/emission of phonons, whereas at low temperatures the electron-electron relaxation times decay similarly to  $T^2$  [7, 10, 44].

## V. ACKNOWLEDGEMENTS

J.B. is supported by FPU grant FPU20/01087. A.C. acknowledges financial support from the Ministerio de Ciencia e Innovación through the grant PID2021-127240NB-I00 and the Ramón y Cajal program through the grant No. RYC2018- 023938-I.

- 
- [1] R. Gurzhi, Minimum of Resistance in Impurity-free Conductors, *J. Exp. Theor. Phys.* **44**, 771 (1963).
- [2] R. Gurzhi, Hydrodynamic effects in solids at low temperature, *Soviet Physics Uspekhi* **11**, 255 (1968).
- [3] P. J. Moll, P. Kushwaha, N. Nandi, B. Schmidt, and A. P. Mackenzie, Evidence for hydrodynamic electron flow in  $\text{PdCoO}_2$ , *Science* **351**, 1061 (2016).
- [4] J. Gooth, F. Menges, N. Kumar, V. Süß, C. Shekhar, Y. Sun, U. Drechsler, R. Zierold, C. Felser, and B. Gotsmann, Thermal and electrical signatures of a hydrodynamic electron fluid in Tungsten Diphosphide, *Nature communications* **9**, 1 (2018).
- [5] A. Jaoui, B. Fauqué, C. W. Rischau, A. Subedi, C. Fu, J. Gooth, N. Kumar, V. Süß, D. L. Maslov, C. Felser, *et al.*, Departure from the Wiedemann-Franz law in  $\text{WP}_2$  driven by mismatch in T-square resistivity prefactors, *npj Quantum Materials* **3**, 1 (2018).
- [6] C. Fu, S. N. Guin, T. Scaffidi, Y. Sun, R. Saha, S. J. Watzman, A. K. Srivastava, G. Li, W. Schnelle, S. S. Parkin, *et al.*, Largely suppressed magneto-thermal conductivity and enhanced magneto-thermoelectric properties in  $\text{PtSn}_4$ , *Research* **2020** (2020).
- [7] U. Vool, A. Hamo, G. Varnavides, Y. Wang, T. X. Zhou, N. Kumar, Y. Dovzhenko, Z. Qiu, C. A. Garcia, A. T. Pierce, *et al.*, Imaging phonon-mediated hydrodynamic flow in  $\text{WTe}_2$ , *Nature Physics* **17**, 1216 (2021).
- [8] G. B. Osterhoudt, Y. Wang, C. A. Garcia, V. M. Plisson, J. Gooth, C. Felser, P. Narang, and K. S. Burch, Evidence for dominant phonon-electron scattering in weyl semimetal  $\text{WP}_2$ , *Physical Review X* **11**, 011017 (2021).
- [9] R. A. Robinson, L. Min, S. H. Lee, P. Li, Y. Wang, J. Li, and Z. Mao, Large violation of the Wiedemann-Franz law in Heusler, ferromagnetic, Weyl semimetal  $\text{Co}_2\text{MnAl}$ , *Journal of Physics D: Applied Physics* **54**, 454001 (2021).

- [10] J. Coulter, R. Sundararaman, and P. Narang, Microscopic origins of hydrodynamic transport in the type-II Weyl semimetal WP<sub>2</sub>, *Phys. Rev. B* **98**, 115130 (2018).
- [11] C. A. C. Garcia, D. M. Nenno, G. Varnavides, and P. Narang, Anisotropic phonon-mediated electronic transport in chiral Weyl semimetals, *Phys. Rev. Materials* **5**, L091202 (2021).
- [12] A. Lavasani, D. Bulmash, and S. Das Sarma, Wiedemann-franz law and fermi liquids, *Phys. Rev. B* **99**, 085104 (2019).
- [13] F. Buccheri, A. De Martino, R. G. Pereira, P. W. Brouwer, and R. Egger, Phonon-limited transport and Fermi arc lifetime in weyl semimetals, *Phys. Rev. B* **105**, 085410 (2022).
- [14] A. Levchenko and J. Schmalian, Transport properties of strongly coupled electron-phonon liquids, *Annals of Physics* **419**, 168218 (2020).
- [15] X. Huang and A. Lucas, Electron-phonon hydrodynamics, *Phys. Rev. B* **103**, 155128 (2021).
- [16] D. T. Son and P. Surowka, Hydrodynamics with triangle anomalies, *Physical review letters* **103**, 191601 (2009).
- [17] M. Isachenkov and A. Sadofyev, The chiral magnetic effect in hydrodynamical approach, *Physics Letters B* **697**, 404 (2011).
- [18] A. Lucas, R. A. Davison, and S. Sachdev, Hydrodynamic theory of thermoelectric transport and negative magnetoresistance in weyl semimetals, *Proceedings of the National Academy of Sciences* **113**, 9463 (2016).
- [19] V. Galitski, M. Kargarian, and S. Syzranov, Dynamo effect and turbulence in hydrodynamic weyl metals, *Physical review letters* **121**, 176603 (2018).
- [20] E. V. Gorbar, V. A. Miransky, I. A. Shovkovy, and P. O. Sukhachov, Consistent hydrodynamic theory of chiral electrons in weyl semimetals, *Phys. Rev. B* **97**, 121105 (2018).
- [21] E. Gorbar, V. Miransky, I. Shovkovy, and P. Sukhachov, Hydrodynamic electron flow in a weyl semimetal slab: Role of chern-simons terms, *Physical Review B* **97**, 205119 (2018).
- [22] P. O. Sukhachov, E. Gorbar, I. A. Shovkovy, and V. Miransky, Collective excitations in weyl semimetals in the hydrodynamic regime, *Journal of Physics: Condensed Matter* **30**, 275601 (2018).
- [23] P. O. Sukhachov and B. Trauzettel, Anomalous gurzhi effect, *Phys. Rev. B* **105**, 085141 (2022).
- [24] S. Zhu, G. Bednik, and S. Syzranov, Weyl hydrodynamics in a strong magnetic field, *Phys. Rev. B* **105**, 125132 (2022).
- [25] P. Matus, R. M. Dantas, R. Moessner, and P. Surówka, Skin effect as a probe of transport regimes in weyl semimetals, *Proceedings of the National Academy of Sciences* **119**, e2200367119 (2022).
- [26] A. A. Burkov and L. Balents, Weyl semimetal in a topological insulator multilayer, *Phys. Rev. Lett.* **107**, 127205 (2011).
- [27] G. B. Halász and L. Balents, Time-reversal invariant realization of the Weyl semimetal phase, *Phys. Rev. B* **85**, 035103 (2012).
- [28] B. Peng, H. Zhang, H. Shao, H. Lu, D. W. Zhang, and H. Zhu, High thermoelectric performance of weyl semimetal taas, *Nano Energy* **30**, 225 (2016).
- [29] Y.-B. Cheng, Q. Li, and J. Zhou, First-principles study on the lattice thermal conductivity of layered dirac semimetal ben4, *Physica E: Low-dimensional Systems and Nanostructures* **147**, 115571 (2023).
- [30] M. A. Stephanov and Y. Yin, Chiral kinetic theory, *Phys. Rev. Lett.* **109**, 162001 (2012).
- [31] D. T. Son and N. Yamamoto, Berry curvature, triangle anomalies, and the chiral magnetic effect in fermi liquids, *Phys. Rev. Lett.* **109**, 181602 (2012).
- [32] L. Onsager, Reciprocal relations in irreversible processes. I., *Phys. Rev.* **37**, 405 (1931).
- [33] J. M. Ziman, *Electrons and phonons: the theory of transport phenomena in solids*, International series of monographs on physics (Clarendon Press, Oxford, 1960).
- [34] P. Arnold, G. D. Moore, and L. G. Yaffe, Transport coefficients in high temperature gauge theories (I): leading-log results, *Journal of High Energy Physics* **2000**, 001 (2000).
- [35] L. Fritz, J. Schmalian, M. Müller, and S. Sachdev, Quantum critical transport in clean graphene, *Phys. Rev. B* **78**, 085416 (2008).
- [36] See supplementary material.
- [37] A. H. MacDonald, R. Taylor, and D. J. W. Geldart, Umklapp electron-electron scattering and the low-temperature electrical resistivity of the alkali metals, *Phys. Rev. B* **23**, 2718 (1981).
- [38] C. Kumar, J. Birkbeck, J. A. Sulpizio, D. Perello, T. Taniguchi, K. Watanabe, O. Reuven, T. Scaffidi, A. Stern, A. K. Geim, and S. Ilani, Imaging hydrodynamic electrons flowing without Landauer-Sharvin resistance, *Nature* **609**, 276 (2022).
- [39] A. Stern, T. Scaffidi, O. Reuven, C. Kumar, J. Birkbeck, and S. Ilani, How electron hydrodynamics can eliminate the Landauer-Sharvin resistance, *Phys. Rev. Lett.* **129**, 157701 (2022).
- [40] S. Li and D. L. Maslov, Lorentz ratio of a compensated metal, *Phys. Rev. B* **98**, 245134 (2018).
- [41] P. Li, Y. Wen, X. He, Q. Zhang, C. Xia, Z.-M. Yu, S. A. Yang, Z. Zhu, H. N. Alshareef, and X.-X. Zhang, Evidence for topological type-ii weyl semimetal wte2, *Nature communications* **8**, 2150 (2017).
- [42] S. Han, Q. Tang, H. Yuan, Y. Luo, and H. Liu, Effects of electron-phonon coupling on the phonon transport properties of the weyl semimetals nbas and taas: A comparative study, *Journal of Materiomics* (2022).
- [43] S. Das Sarma, E. H. Hwang, and H. Min, Carrier screening, transport, and relaxation in three-dimensional dirac semimetals, *Phys. Rev. B* **91**, 035201 (2015).
- [44] C. A. Garcia, D. M. Nenno, G. Varnavides, and P. Narang, Anisotropic phonon-mediated electronic transport in chiral weyl semimetals, *Physical Review Materials* **5**, L091202 (2021).
- [45] P. Coleman, *Introduction to Many-Body Physics* (Cambridge University Press, 2015).

## Appendix A: Hamiltonian and Scattering Amplitudes

As mentioned in the main text, a two-band Hamiltonian matrix of the form

$$\mathcal{H}_0(\mathbf{p}) = \mathbf{d}(\mathbf{p}) \cdot \boldsymbol{\sigma}, \quad (\text{A1})$$

where  $\mathbf{d} = (d_1, d_2, d_3)^T$  has positive and negative energy  $\epsilon_{\pm, \mathbf{p}} = \pm d(\mathbf{p}) \equiv \pm \sqrt{\mathbf{d}^2(\mathbf{p})}$  eigenstates, which are respec-

tively given by ( $c \leftrightarrow +$ ,  $v \leftrightarrow -$ )

$$|+\mathbf{p}\rangle \equiv \frac{1}{\sqrt{2d(d+d_3)}} \begin{pmatrix} d+d_3 \\ d_1+id_2 \end{pmatrix}, \quad (\text{A2})$$

$$|-\mathbf{p}\rangle \equiv \frac{1}{\sqrt{2d(d+d_3)}} \begin{pmatrix} d_1-id_2 \\ -d-d_3 \end{pmatrix}, \quad (\text{A3})$$

where  $c$  stands for conduction band ( $+d(\mathbf{p})$ ) and  $v$  for valence band ( $-d(\mathbf{p})$ ). The particle fermion operators are related to the original fermion operators by the unitary transformation  $\psi_{\mathbf{p}} = U_{\mathbf{p}} c_{\mathbf{p}}$ , where  $U_{\mathbf{p}} \equiv (|+\mathbf{p}\rangle, |-\mathbf{p}\rangle)$ . In the particle-hole basis, the electron-phonon interaction given by the deformation potential (4) becomes

$$H_{\text{e-ph}} = \int_{\mathbf{p}', \mathbf{p}, \mathbf{q}} g_{\mathbf{p}', \mathbf{p}}^{\mathbf{q}} (a_{\mathbf{q}} + a_{\mathbf{q}}^{\dagger}) c_{\mathbf{p}'}^{\dagger} U_{\mathbf{p}'}^{\dagger} U_{\mathbf{p}} c_{\mathbf{p}} \delta^{(3)}(\mathbf{p}' - \mathbf{p} - \mathbf{q}), \quad (\text{A4})$$

For  $\mu \gg T$ , the effects of the negative energy band are exponentially suppressed, so we ignore its effects from now on. For the fermion-phonon interaction, it implies

that we only consider care about the term proportional to  $c_{+, \mathbf{p}}^{\dagger} c_{+, \mathbf{p}}$ , hence the effective fermion coupling to the relevant fermion sector is given by the expression given in (6), i.e.

$$g_{\mathbf{p}', \mathbf{p}}^{\text{eff } \mathbf{q}} \equiv g_{\mathbf{p}', \mathbf{p}}^{\mathbf{q}} \langle +\mathbf{p} | +\mathbf{p}' \rangle, \quad (\text{A5})$$

where for simplicity of notation we have used the label  $u_{\mathbf{p}} \equiv u_{+, \mathbf{p}}$ , and will continue to do so henceforth. The scattering amplitude for fermion collisions with incoming momenta  $\mathbf{p}, \mathbf{k}$  and outgoing momenta  $\mathbf{p}', \mathbf{k}'$  mediated by virtual phonons is given by the interference of the  $t$  and  $u$  channels,  $M = A_t - A_u$

$$A_t = -g_{\mathbf{p}', \mathbf{p}}^{\mathbf{q}} g_{\mathbf{k}, \mathbf{k}'}^{\mathbf{q}} \mathcal{D}(\mathbf{q}, \omega) \langle +\mathbf{p}' | +\mathbf{p} \rangle \langle -\mathbf{k}' | -\mathbf{k} \rangle, \quad (\text{A6})$$

where  $\mathbf{q} = \mathbf{p}' - \mathbf{p}$  and  $\omega = d(\mathbf{p}') - d(\mathbf{p})$ . The amplitude for the  $u$  channel  $A_u$  is obtained by exchanging  $\mathbf{p}' \leftrightarrow \mathbf{k}'$  in the expression for  $A_t$ . The square of the amplitude relevant for the Boltzmann equation can be shown then to be

$$\begin{aligned} |M|^2(\mathbf{p}, \mathbf{k}, \mathbf{p}', \mathbf{k}') &= |A_t|^2 + |A_u|^2 - 2\text{Re}[A_t^* A_u] = \\ &\left\{ |\mathcal{D}|^2(\mathbf{q}_t, \omega_t) |g_{\mathbf{p}', \mathbf{p}}^{\mathbf{q}_t} g_{\mathbf{k}, \mathbf{k}'}^{\mathbf{q}_t}|^2 - \text{Re}[\mathcal{D}^*(\mathbf{q}_t, \omega_t) \mathcal{D}(\mathbf{q}_u, \omega_u)] g_{\mathbf{p}', \mathbf{p}}^{\mathbf{q}_t} g_{\mathbf{k}, \mathbf{k}'}^{\mathbf{q}_t} g_{\mathbf{k}', \mathbf{p}}^{\mathbf{q}_u} g_{\mathbf{k}, \mathbf{p}'}^{\mathbf{q}_u} \right\} [1 + \hat{\mathbf{d}}(\mathbf{p}) \cdot \hat{\mathbf{d}}(\mathbf{p}')] [1 + \hat{\mathbf{d}}(\mathbf{k}) \cdot \hat{\mathbf{d}}(\mathbf{k}')] \\ &+ \left\{ |\mathcal{D}|^2(\mathbf{q}_u, \omega_u) |g_{\mathbf{k}', \mathbf{p}}^{\mathbf{q}_u} g_{\mathbf{k}, \mathbf{p}'}^{\mathbf{q}_u}|^2 - \text{Re}[\mathcal{D}^*(\mathbf{q}_t, \omega_t) \mathcal{D}(\mathbf{q}_u, \omega_u)] g_{\mathbf{p}', \mathbf{p}}^{\mathbf{q}_t} g_{\mathbf{k}, \mathbf{k}'}^{\mathbf{q}_t} g_{\mathbf{k}', \mathbf{p}}^{\mathbf{q}_u} g_{\mathbf{k}, \mathbf{p}'}^{\mathbf{q}_u} \right\} [1 + \hat{\mathbf{d}}(\mathbf{p}) \cdot \hat{\mathbf{d}}(\mathbf{k}')] [1 + \hat{\mathbf{d}}(\mathbf{k}) \cdot \hat{\mathbf{d}}(\mathbf{p}')] \\ &+ \text{Re}[\mathcal{D}^*(\mathbf{q}_t, \omega_t) \mathcal{D}(\mathbf{q}_u, \omega_u)] g_{\mathbf{p}', \mathbf{p}}^{\mathbf{q}_t} g_{\mathbf{k}, \mathbf{k}'}^{\mathbf{q}_t} g_{\mathbf{k}', \mathbf{p}}^{\mathbf{q}_u} g_{\mathbf{k}, \mathbf{p}'}^{\mathbf{q}_u} [1 - \hat{\mathbf{d}}(\mathbf{p}) \cdot \hat{\mathbf{d}}(\mathbf{k}')] [1 - \hat{\mathbf{d}}(\mathbf{p}') \cdot \hat{\mathbf{d}}(\mathbf{k}')]. \end{aligned} \quad (\text{A7})$$

Following the discussion of the main text, a distinction between the behavior at high and low temperatures can be made so as to simplify (A7). At high temperatures  $T \gg T_{\text{BG}}$ , the interference terms can be dropped. In addition, since the collision integral is symmetric with the exchange  $\mathbf{p}' \leftrightarrow \mathbf{k}'$ , inside the collision integral one effectively has that  $|A_t|^2 = |A_u|^2$ .

At low temperatures  $T \ll T_{\text{BG}}$ , the  $\omega$  dependence of the phonon propagators can be dropped at the lowest order in  $\omega/\omega_{\mathbf{q}}$  expansion. The small linewidth can be dropped as well, leading to the cancellation of the first two terms in (A7). All in all, these considerations lead to the square scattering amplitudes

$$|M|_{\text{h.t.}}^2(\mathbf{p}, \mathbf{k}, \mathbf{p}', \mathbf{k}') = \frac{2U^2}{4} \left| \frac{q^2}{\omega^2 - \omega_{\mathbf{q}}^2 + i\omega_{\mathbf{q}}\Gamma_{\mathbf{q}}} \right|^2 [1 + \hat{\mathbf{d}}(\mathbf{p}) \cdot \hat{\mathbf{d}}(\mathbf{p}')] [1 + \hat{\mathbf{d}}(\mathbf{k}) \cdot \hat{\mathbf{d}}(\mathbf{k}')], \quad (\text{A8})$$

$$|M|_{\text{l.t.}}^2(\mathbf{p}, \mathbf{k}, \mathbf{p}', \mathbf{k}') = \frac{U^2}{4c^4} [1 - \hat{\mathbf{d}}(\mathbf{p}) \cdot \hat{\mathbf{d}}(\mathbf{k}')] [1 - \hat{\mathbf{d}}(\mathbf{p}') \cdot \hat{\mathbf{d}}(\mathbf{k}')], \quad (\text{A9})$$

where the labels "h.t." and "l.t." stand are for high temperatures and low temperatures, respectively. The ex-

PLICIT forms of the electron-phonon coupling (5) and the phonon propagator (7) have been used.

## Appendix B: Phonon Linewidth

Considering only intravalley interactions, the phonon linewidth is calculated from the first diagram in Fig. 1 of the main text. To do so, one calculates the self-energy,

$$\Sigma(\mathbf{q}, i\omega_n) = \beta^{-1} \int_{\mathbf{p}} \sum_{i\nu_m} \left( i g_{\mathbf{p}', \mathbf{p}}^{\text{eff } \mathbf{q}} \right) \left( i g_{\mathbf{p}', \mathbf{p}}^{\text{eff } \mathbf{q}^*} \right) \mathcal{G}_0(\mathbf{k}, i\nu_m) \mathcal{G}_0(\mathbf{k} + \mathbf{q}, i\nu_m + i\omega_n) \quad (\text{B1})$$

$$= -\beta^{-1} \int_{\mathbf{p}} \sum_{i\nu_m} (g_{\mathbf{p}', \mathbf{p}}^{\mathbf{q}})^2 \frac{|\langle +\mathbf{p} | +\mathbf{p}' \rangle|^2}{[i\nu_m + p_f - p][i\nu_m + i\omega_n + p_f - p']} = \int_{\mathbf{p}} (g_{\mathbf{p}', \mathbf{p}}^{\mathbf{q}})^2 |\langle +\mathbf{p} | +\mathbf{p}' \rangle|^2 \frac{f_0(p) - f_0(p')}{i\omega_n + p - p'}. \quad (\text{B2})$$

where  $\mathbf{p}' = \mathbf{p} + \mathbf{q}$  and the Matsubara sum has been performed in the last equality. After analytically continuing to real frequencies  $i\omega_n \rightarrow \omega - i\delta$ , the phonon linewidth can be obtained

$$\Gamma_{\mathbf{q}}^{\text{e-ph}} \equiv 2\text{Im} \{ \Sigma(\mathbf{q}, \omega_{\mathbf{q}} - i\delta) \} = (2\pi) \int_{\mathbf{p}} (g_{\mathbf{p}', \mathbf{p}}^{\mathbf{q}})^2 |\langle +\mathbf{p} | +\mathbf{p}' \rangle|^2 [f_0(p) - f_0(p')] \delta(p' - p - \omega_{\mathbf{q}}), \quad (\text{B3})$$

where we have used the Cauchy-Dirac relation  $\frac{1}{x-a-i\delta} = P\frac{1}{x-a} + i\pi\delta(x-a)$ . Note that the structure factor is given by

$$|\langle +\mathbf{p} | +\mathbf{p}' \rangle|^2 = \frac{1 + \hat{\mathbf{d}}(\mathbf{p}) \cdot \hat{\mathbf{d}}(\mathbf{p}')}{2}. \quad (\text{B4})$$

We will also use the approximation where

$$f_0(p) - f_0(p') \approx \omega_{\mathbf{q}} [-f'_0(p)] \approx \omega_{\mathbf{q}} \delta(p - p_f), \quad (\text{B5})$$

where the first equality comes from  $p, p' \sim p_f \gg cq$  and the latter is the lowest order in the Sommerfeld approximation. The intranode contribution is given by the loop with fermions of the same chirality. After a simple calculation, it can be shown that

$$\Gamma_{\text{e-ph}}^{\text{intra}}(\mathbf{q}) = \begin{cases} 2 \cdot \frac{U}{4\pi} q p_f^2 \left( 1 - \frac{q^2}{4p_f^2} \right), & \text{if } q \leq 2p_f, \\ 0, & \text{if } q > 2p_f. \end{cases} \quad (\text{B6})$$

The leading factor of 2 comes from considering both  $L$  intraband and  $R$  intraband contributions, which are identical. The interband contribution on the other hand can be shown to be

$$\Gamma_{\text{e-ph}}^{\text{inter}}(\mathbf{q}) = \begin{cases} \frac{U}{4\pi} \frac{q^2}{|\mathbf{q}-2\mathbf{b}|} p_f^2 \left[ 1 - \frac{|\mathbf{q}-2\mathbf{b}|^2}{4p_f^2} + \frac{|\mathbf{q}-2\mathbf{b}|^2}{2p_f^2} \cos^2 \theta_{b, \mathbf{q}-2\mathbf{b}} - \left( 1 - \frac{|\mathbf{q}-2\mathbf{b}|^2}{4p_f^2} \right) \frac{\sin^2 \theta_{b, \mathbf{q}-2\mathbf{b}}}{2} \right], & \text{if } |\mathbf{q}-2\mathbf{b}| \leq 2p_f, \\ 0, & \text{if } |\mathbf{q}-2\mathbf{b}| > 2p_f. \end{cases} \quad (\text{B7})$$

The calculation of these linewidths is similar to the calculation of the collision matrix terms for phonon absorption and emission by fermions provided in the next section, so we refer the reader to it for more detail. The full linewidth is simply given by

$$\Gamma_{\mathbf{q}}^{\text{e-ph}} = \Gamma_{\text{e-ph}}^{\text{intra}}(\mathbf{q}) + \Gamma_{\text{e-ph}}^{\text{inter}}(\mathbf{q}). \quad (\text{B8})$$

## Appendix C: Electron-Phonon Coupling

The electron-phonon coupling strength is usually parameterized [45] in terms of the dimensionless

$$\lambda = \frac{1}{\pi} \int_{\mathbf{p}} \delta(\varepsilon_{\mathbf{p}} - \mu) \int_{\mathbf{q}} \frac{\Gamma_{\mathbf{q}}^{\text{e-ph}}}{\omega_{\mathbf{q}}^2}. \quad (\text{C1})$$

The integral can be evaluated using the phonon linewidths for intraband (B6) and interband scattering

(B7) using (B8). This in turn gives

$$\lambda = \frac{5U p_f^2}{6\pi^2 c^2} \Rightarrow U p_f^2 = \frac{6\pi^2}{5} \lambda c^2 \sim 12\lambda c^2. \quad (\text{C2})$$

## Appendix D: Numeric Integrals

Several numeric integrals appear often in the calculations and are related to the integrals of momenta that

include the Fermi-Dirac distribution and the Bose Einstein distribution. We list them here for convenience:

$$c_2 = \int_{-\infty}^{\infty} x^2 \frac{e^x}{(1+e^x)^2} = \frac{1}{2} \int_{-\infty}^{\infty} x^2 \frac{e^x}{(1-e^x)^2} = \frac{\pi^2}{3}, \quad (\text{D1})$$

$$b_4 = \int_{-\infty}^{\infty} x^4 \frac{e^x}{(1-e^x)^2} = \frac{4\pi^4}{15}, \quad (\text{D2})$$

$$g_n = \int_{-\infty}^{\infty} dx \frac{e^x}{(e^x+1)^2} [\zeta(n) - \text{Li}_n(-e^{-x})], \quad (\text{D3})$$

where  $g_4 \approx 4.3$ ,  $g_5 \approx 5.2$  and  $g_6 \approx 6.1$ .